# Remote Sounding of the Stratosphere by the Occultation Method: The ORA Experiment

Didier Fussen, Filip Vanhellemont, and Christine Bingen

Institut d'Aéronomie Spatiale de Belgique (IASB), 3, avenue Circulaire, B 1180 Bruxelles BELGIUM E-Mail: Didier.Fussen@oma.be

**Abstract.** The occultation technique is based on recording of the sun light above the horizon. Its benefit resides in the derivation of an absolute quantity (the slant path optical thickness) through the measurement of a relative signal. The ORA experiment is presented together with the inversion method used to retrieve the atmospheric components.

## 1 The Occultation Method

The constituents of the Earth's atmosphere can be monitored from in situ measurements and by remote sounding from ground-based instruments or by satellite borne spectrometers. However, only systematic measurements from low orbit spacecrafts are susceptible to give a good global coverage in a minimal temporal window.

In the case of a heliosynchroneous orbit (where the orbital plane rotates with a precession velocity of 1 degree per day), an altitude of about 800 km allows a 3-day subcycle that makes nadir looking instruments to fully cover the globe. Although nadir looking instruments can achieve very high horizontal resolutions, they suffer from two major drawbacks: they can only measure integrated column densities in the UV-visible range and they require a calibration procedure in order to correctly interpret the observed absolute radiances.

Both difficulties are actually solved by using the occultation technique as explained in the pioneering article of [11]. The principle of occultation is quite simple. When a source of light (Sun, Moon, a planet or a star) is high above the horizon, the light spectrum of the source is recorded by a spectrometer. The measured intensities (at different wavelengths) correspond to light rays that have not been attenuated by the atmosphere. During the orbital movement, the instrument observes a relative setting of the celestial body through the Earth's atmosphere until a complete occultation occurs. A vertical scan of the atmosphere is performed by recording snapshots of the transmitted intensity along the occultation track. Clearly, this allows to achieve a high vertical resolution due to the limb geometry but also to the exponential decrease of gas density profile with altitude. Indeed, most of the slant path optical thickness is concentrated in the neighborhood of the tangent point

Rodolfo Guzzi (Ed.): LNP 607, pp. 242–262, 2003.

(where "tangent point" actually means the point of closest approach with respect to the Earth's surface). An other advantage of the limb viewing over nadir viewing is the much higher sensitivity to trace graces because the integrated number density along the slant path is typically 50 larger than the corresponding vertical column above the tangent point. However, a decisive benefit of the occultation technique resides in the derivation of an absolute quantity (the slant path optical thickness) through the measurement of a relative signal, i.e. the atmospheric transmittance, computed by ratioing the measured intensities, at all wavelengths, with the unattenuated light spectrum measured outside the atmosphere.

## 2 The ORA Experiment

The Occultation RAdiometer (ORA) is a simple UV-visible instrument developed by the Belgian Institute for Space Aeronomy, that was launched in July 1992 on board the EUropean REtrievable CArrier (EURECA) for a 1-year mission. The instrument was dedicated to the measurement of vertical profiles of $O_3$, $NO_2$, $H_2O$ number densities as well as the stratospheric aerosols.

A well known method for the measurement of minor atmospheric constituents is the solar occultation technique, the advantages being mainly the high signal-to-noise ratio and the self-calibration of the instrument since full scale and the zero point are obtained automatically. The carrier being designed for microgravity experiments, moving parts in the instrument had to be limited to a minimum. Therefore, in view of the weight and power budget and considering that the satellite was sun pointing by itself, the ORA instrument had no sun tracking device and observed the full solar disk (see Fig. 1).

ORA recorded 6821 sunsets and sunrises from a circular orbit at an altitude of 508 km. Although the low orbital plane inclination (28°) of the satellite restricted the latitude coverage between 40° S and 40° N (see Fig. 2), the period of measurement was particulary interesting due to the unique opportunity of observing the relaxation of the Mount Pinatubo eruptive perturbations.

The experimental design has been described elsewhere [1]. Briefly, it consists of 8 broadband channels whose nominal wavelengths are presented in Table 1 together with the associated predominant constituents.

The apparent vertical resolution of the instrument appears to be poor (about 25 km, defined by the solar disc size at the tangent point). However the signal-to-noise ratio is very high for the same reason, suggesting that a large information content can be retrieved from the transmission and allowing the achievement of a 2-3 km vertical resolution.

The purpose of this chapter is to present the retrieval algorithm of the ORA experiment. In the first section we will describe the vertical inversion

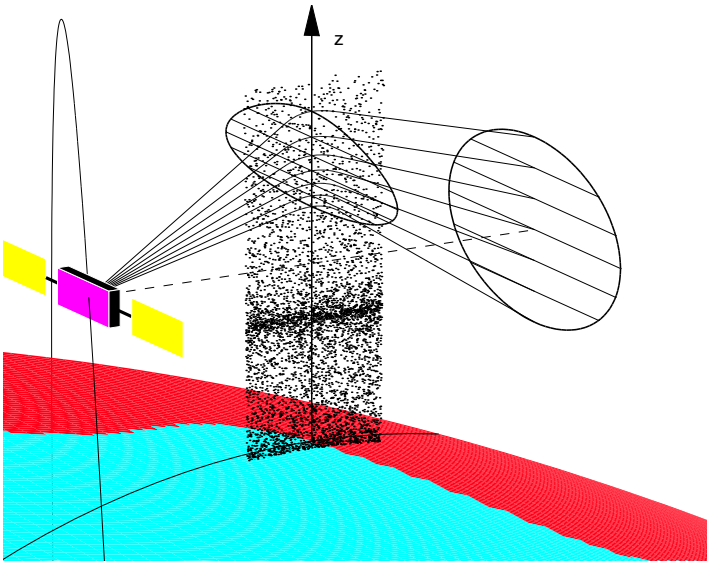


**Fig. 1.** The ORA occultation geometry

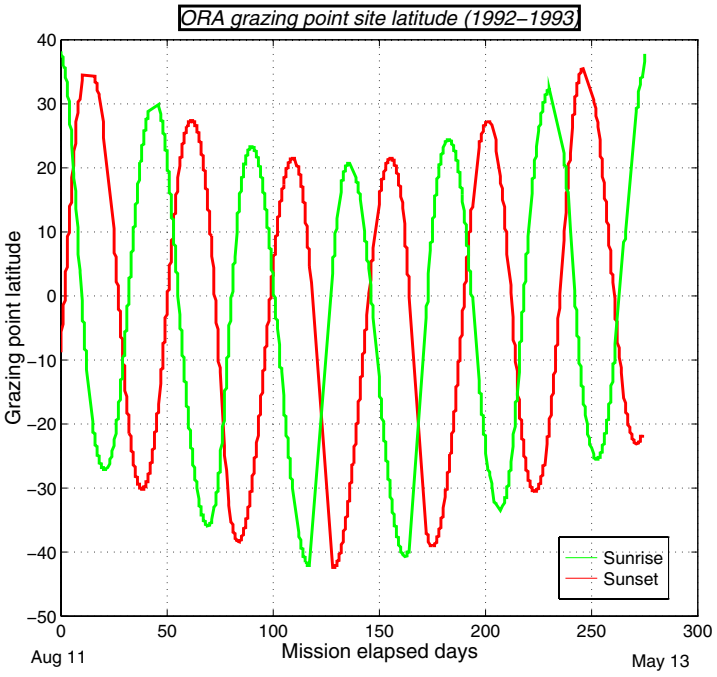


**Fig. 2.** Latitude of tangent point

**Table 1.** Major light absorbers in the different UV/visible/near-IR channels

| Channel number | 7 | 6 | 8 | 2 | 1 | 5 | 4 | 3 |
|---|---|---|---|---|---|---|---|---|
| $\lambda$[nm] | 259 | 340 | 385 | 435 | 442 | 600 | 943 | 1013 |
| predominant | $O_3$ | neutrals | aerosol | aerosol | aerosol | $O_3$ | aerosol | aerosol |
| constituents | neutrals | aerosol | $NO_2$ | $NO_2$ | $NO_2$ | aerosol | $H_2O$ | |

scheme. Then we will discuss the spectral inversion (or separation between the different constituents) as well as the error budget.

## 3 The Vertical Inversion Algorithm

The retrieval of constituent altitude profiles faces two inversion problems: in the vertical inversion, one has to compute the relative contribution of each atmospheric layer to the slant path optical thickness; in the spectral inversion, one performs the separation of different species absorbing light at the same wavelength. The unusual choice of performing the vertical inversion before the spectral inversion was guided by the need to solve the most difficult problem first. Furthermore, the wavelength dependence of aerosol extinction is unknown but varies a priori with altitude. By performing the spectral inversion first, it is only possible to obtain averaged values corresponding to a particular tangent altitude. In the vertical inversion, the atmospheric extinction coefficient is integrated along the line-of-sight but also over the solid angle spanned by the apparent solar disc.

The angular size of the Sun is responsible for smoothing vertical structures out in the recorded transmittance. In Fig. 3 we present the synthetic transmittance produced by a climatological ozone profile when the apparent size of the light source is varied from punctual (like a star) to twice the Sun's size.

At any time during the occultation, the relative transmission of a solar ray, grazing the Earth at an altitude $h$, can be written as:

$$T_\lambda(h) = \exp(-\int_{s1}^{s2} \beta_\lambda(h)\ ds(h)) \tag{1}$$

where $\beta_\lambda(h)$ is the total attenuation coefficient along the optical path whose length element is described by the variable $s(h)$. For any of the channels:

$$\beta_\lambda(h) = \beta_\lambda^{Rayleigh}(h) + \beta_\lambda^{Aerosol}(h) + \beta_\lambda^{O_3}(h) + \ldots \tag{2}$$

where the superscript Rayleigh refers to the the light scattering by the air. The relative signal (with respect to the full Sun) measured by ORA reads:

$$S_\lambda(h) = \int_{\Delta\Omega} W(\Omega)\, T_\lambda(h(\Delta))\, d\Omega \tag{3}$$

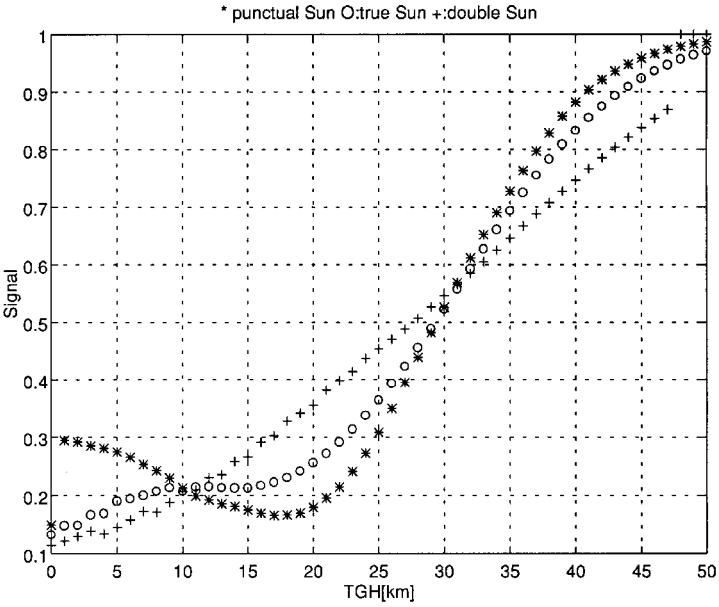


**Fig. 3.** Synthetic transmittance signal for a pure ozone atmosphere at $\lambda = 600$ nm for punctual, normal and doubled Sun size

because the instrument observes the whole solar disk within the solid angle $\Delta\Omega$ spanning more than 25 km in altitude. The angular function $W(\Omega)$ expresses the relative light distribution across the Sun including area and solar limb darkening dependencies. The attenuation coefficient can be expressed as:

$$\beta_{ij}(z) = \sigma_i \; n_j \, (z) \tag{4}$$

for a particular absorber $j$ where $\sigma_i$ represents the attenuation cross section in the channel $i$, and $n_j \, (z)$ the concentration profile of constituent j.

Refraction in the atmosphere actually produces several effects in an occultation experiment. Refraction not only increases the true grazing height $h$ up to 14 km (for a tangent geometrical path), but it also bends the rays (up to 1° i.e., twice the Sun's diameter), shifting the occultation time period (up to 20 s) before geometrical sunrise or after geometrical sunset. Furthermore, the optical path length is increased.

It is a good approximation to consider that the refraction index $N(R)$ has only a radial dependence and that the light trajectory lies in the refraction plane containing the emitter Sun point, the center of the approximating sphere and the satellite. The ray path obeys the following differential equation [2]

$$\frac{dR}{d\theta} = \pm \frac{R}{K} \cdot \sqrt{N^2(R)\, R^2 - K^2} \tag{5}$$

where $\theta$ is the polar angle in the refraction plane and the turning point is defined by $dR/d\theta := 0$. Bouguer's law expresses the momentum conservation as

$$K = \| \overrightarrow{R} \times N \overrightarrow{S} \| = \text{const} \tag{6}$$

where $\overrightarrow{S}$ is the unitary vector tangent to the trajectory. Consequently, the angle defining the penetration of a ray in the atmosphere determines the value of $K$, which in turn, determines the grazing altitude.

Actually, we have a boundary value problem because the position of the satellite is known but not the angle under which the ray enters the instrument. Therefore the full problem has been solved iteratively by a shooting method using a classical Runge-Kutta scheme with variable step size to integrate equation(5) [10]. in the absorbing medium.

The atmosphere can be viewed as a kind of diverging lens [7] where the bending of the rays increases (however, not linearly) as they get closer to the surface. The image of the Sun through the atmosphere is consequently affected by refraction because rays coming from the "bottom" are more refracted than those coming from the "top", which results in Sun flattening (typical values are 15% at 30 km, 38% at 20 km, and 69% at 10 km). Sun flattening is also associated with a less intuitive phenomenon: the refractive dilution effect [6]. This means that the energy flux reaching the detector will be proportional to the apparent size of the source.

Taking into account refractive effects and solar limb darkening, the inversion problem of retrieving the vertical extinction profile gets quite complicated and is highly non-linear. There are well known published algorithms for addressing the problem of inverting slant path optical thicknesses recorded during a solar occultation. The classical onion peeling method is clearly inadequate due to the collective contribution of a large altitude range to the signal. The Chahine algorithm used in SAGE II [4, 9] was also tested but turned out to become unstable (wavy spurious structures appeared) beyond an optimal number of iterations which is a priori difficult to determine and somewhat arbitrary. Optimal estimation methods [12] were also considered but the impact of the high non-linearity of the problem in a bayesian approach was expected to perturb the error analysis whose simplicity is a major advantage of this formalism. Also, the absence of validated climatologies concerning the covariance matrix of the altitude profiles of the aerosol extinction was judged to be a large uncertainty factor in defining the a priori state vector after a major volcanic eruption.

In a first publication [6], we presented the method of a Natural Orthogonal Polynomial Expansion (NOPE) as a useful tool for describing the total extinction profile $\beta(z)$ (expressed in $\mathrm{m}^{-1}$ units) as:

$$\beta(z) = \beta_0(z) \sum_{i=0}^{n} \alpha_i \; P_i(z) \tag{7}$$

where $\beta_0(z)$ stands for a reasonable a priori profile. The family of orthogonal polynomials $P_i(z)$ is numerically generated, using the Stieltjes procedure. Finally, the merit function comparing the squared difference between the modelled transmission and the observed one is minimized with respect to the $\alpha_i$ coefficients, using a Levenberg-Marquardt algorithm (see Fig. 4).

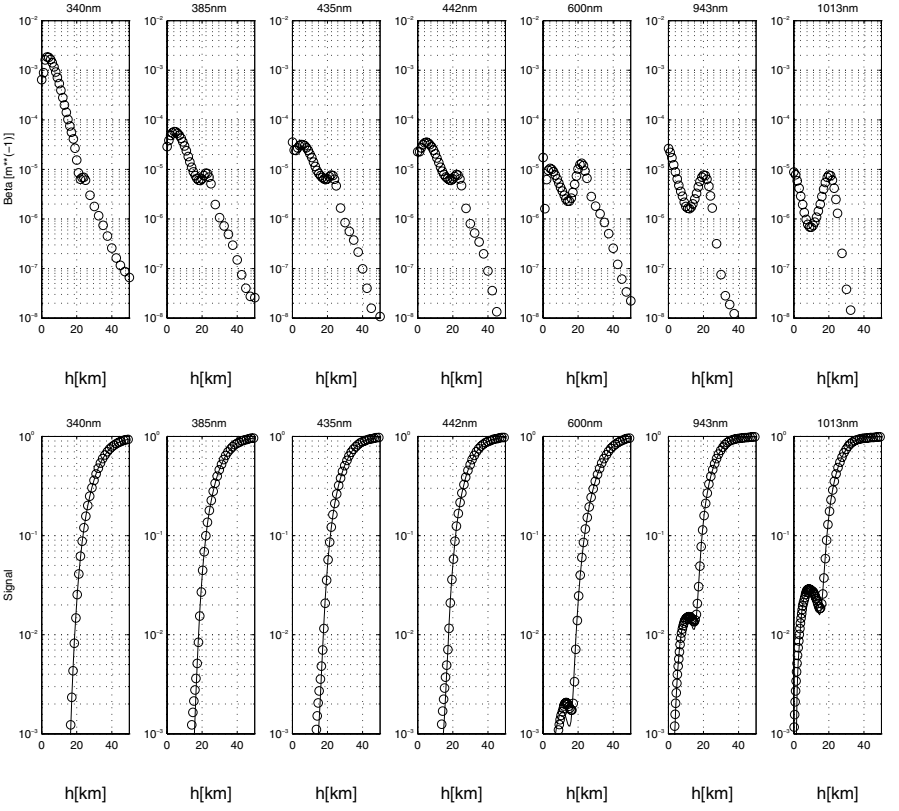


**Fig. 4.** Top: Retrieved profiles in ORA channels by the NOPE method. Bottom: Corresponding measured (full line) and computed (circles) transmittances

In a recent publication [5], we have validated the whole algorithm by comparing about 25 coincident ORA and SAGE II[4] total extinction profiles for 3 common spectral channels ($\lambda = 385, 600, 1020$nm). The agreement was acceptable (typically 20 % in the 15-40 km altitude range), proving that the method is able to retrieve small to medium scale vertical structures (2-5 km), much smaller than the Sun's apparent size. However, the ORA profiles turned out to be slightly oversmoothed with respect to SAGE because they are constructed on a basis of continuous functions. A second limitation of the method was the possible although not systematical appearance of a more chaotic pro-

file behaviour above 35 km and below 15 km where the transmission signal respectively approaches 1 (small optical thickness) or 0 (saturation regime). The problem was clearly identified as cancellation effects in the $\alpha_i$ coefficients enhanced by the important redundancy between two transmissions recorded at two neighboring tangent altitudes (for which there is a large overlap between the corresponding apparent solar disks). However, increasing the size $n$ (normally having the value of 10) of the basis was inefficient due to the complicated and flat topology around the merit function minimum.

Preliminary spectral inversion of the retrieved total extinction profiles showed, in the mentioned altitude range, the high sensitivity of the results to the more chaotic part of the extinction profile. On the other hand, looking at the residual (typically $2.10^{-3}$) of the vertical inversion merit function, it was clear that this residual was an oscillating but smooth function of altitude, well above the noise level of the instrument.

As no more information could be extracted from the inversion of one occultation by the NOPE method, we decided to increase the information content by using a large subset of inverted profiles to construct a geometric 'direct method' (DM) capable of producing more robust profiles in the low and high altitude regions.

In Fig. 5, we represent a schematic view of the occultation geometry. It is clear that the main contribution to the slant-path optical thickness comes from a limited region of length $S$ (about 500 km for Rayleigh scattering) surrounding the tangent point. The transmitted signal at satellite position 2 is therefore mainly influenced by the value of the total extinction at $z = h$ and also by all rays issued from the altitudes ranging approximately from $h_{\min}$ to $h_{\max}$. Inversely, it is natural to consider that the value of the total extinction at $z = h$ can be formally determined from the evolution of the total transmission between points 1 and 3.

Using a scale factor ($S = 500$ km) for the optical path, we express $\beta(z)$ as:

$$\beta(z) = \frac{-\ln(y)}{S} + \beta^R_{\min}(z) \tag{8}$$

where

$$y = y(z) = \frac{1}{2}\left(\tanh\left(\zeta\,(z) - \frac{1}{2}\right) + 1\right) \tag{9}$$

$$\zeta\,(z) = \int_{h_{\min}(z)}^{h_{\max}(z)} f\,(h; z)\;\; T(h)\; dh \tag{10}$$

where $f\,(h; z)$ is an unknown function weighting the measured transmittance $T(h)$ along the nominal tangent altitude $h$. The latter equation defines $\zeta\,(z)$ as a weighted sum of the transmission values contributing to the value of $\beta(z)$. The non-linear transformation of (9) has the property of constraining the effective transmission $y(z)$ to range between 0 and 1. In (8), we decided to constrain the total extinction coefficient to be greater or equal to a minimal

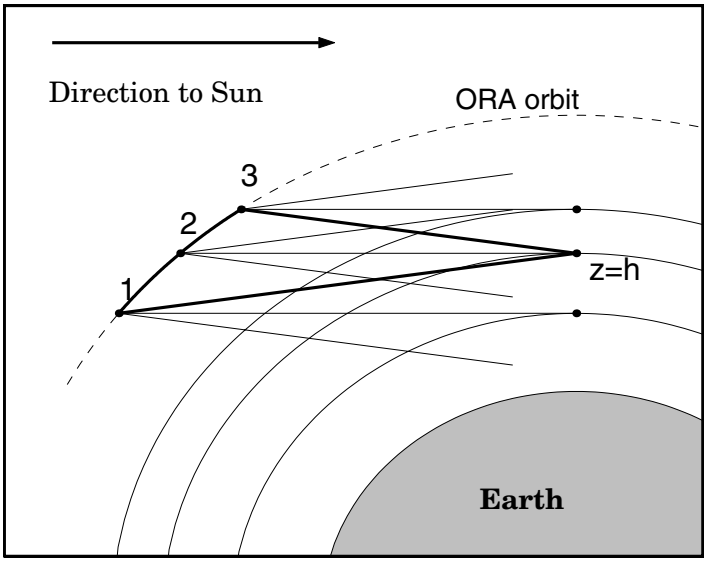


**Fig. 5.** Schematic view of the geometrical content of the Direct Method. The extinction at $z = h$ is mainly determined by transmittance between points 1 and 3

value acceptable for the Rayleigh extinction coefficient. Finally, we introduce the change of variable:

$$x(h) = \frac{(h - h_{\min}(z))}{\Delta h} - 1 \;\; with\; \Delta h \equiv \frac{(h_{\max}(z) - h_{\min}(z))}{2} \tag{11}$$

One gets:

$$\zeta\,(z) = \int_{-1}^{1} f(h(x); z)\; T(h(x))\; dx \tag{12}$$

The weighting function $f(h(x); z)$ is developed, for any altitude $z$, on a basis of the first eleven Chebyshev polynomials as

$$f(x, z) = \sum_{j=0}^{10} a_j(z)\;\; \cos(j \arccos(x)) \tag{13}$$

After algebraic inversion of equations 8, 9 and 10, the determination of the $a_j(z)$ coefficients has been performed using a linear least-squares procedure over the results of 1000 occultations vertically inverted by using the NOPE method and the error on $\beta(z)$ was estimated from the associated covariance matrix and standard error propagation (the ORA error characterization has been discussed in [5]).

In Fig. 6, we present a typical result of both NOPE and DM methods. In the upper part of the figure, the NOPE total extinction profile at

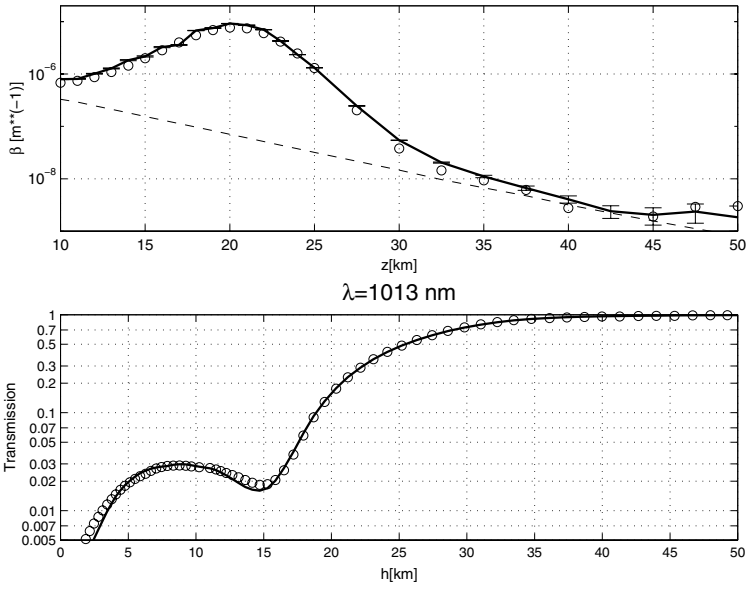


**Fig. 6.** Top: NOPE total extinction (circles) and corrected DM profiles (full lines). The dashed lines represent Rayleigh extinction. Bottom: Measured transmission (full lines) and modelled NOPE transmission (circles).

$\lambda = 1013$ nm is reported by circles. At $\lambda = 1013$ nm, some erratic behaviour occurs above 40 km. Note, however, the large dynamic range of the profile. In the lower part of the figure, the associated best fit transmission is plotted against the measured transmission. A close examination reveals that the modelled transmission in the NOPE method does not perfectly fit the dip at 15 km associated with the Junge layer maximum at 20 km. Below 5 km, the NOPE transmission seems to be slightly overestimated. All these effects seem to have been ameliorated by the application of the DM method which does not introduce a large correction at altitudes between 2 km and 40 km, as we would expect for consistency. Below 20 km, where the transmission is almost zero, the total extinction receives extra stabilisation. It is worth noting that the results of the DM method are independently computed for each event and for each altitude from the raw normalized transmission even if the used coefficients $a_j(z)$ were determined by using a large statistics of occultations.

What is the vertical resolution of the ORA instrument? A good description of the error analysis formalism may be found in [13] where the matrix of averaging kernels $\Phi$ relates the a priori profile $\beta_0(z)$, the retrieved profile $\beta(z)$ and the true profile $\beta_t(z)$ through the relation:

$$(\beta(z) - \beta_0(z)) = \Phi \cdot (\beta_t(z) - \beta_0(z)) \tag{14}$$

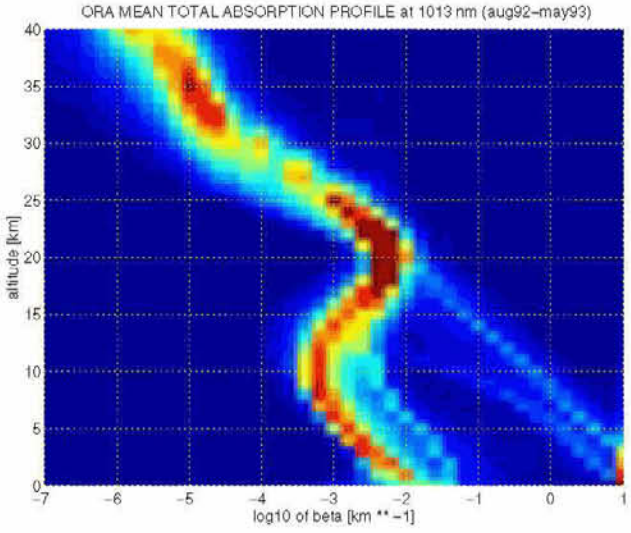


**Fig. 7.** Altitude histogram of the extinction profile at 1020 nm

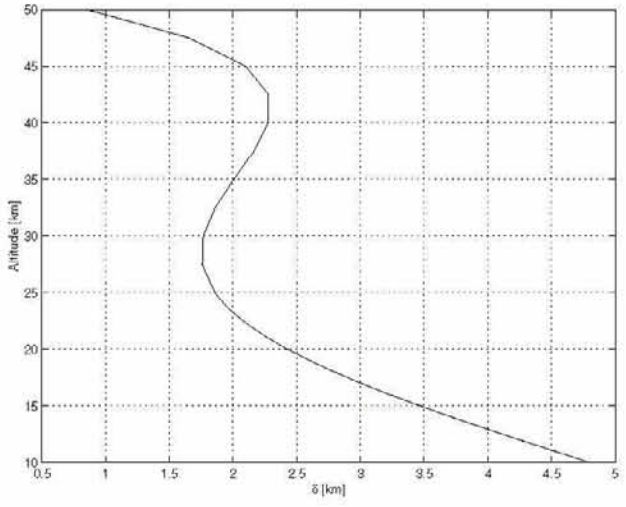


**Fig. 8.** ORA vertical resolution

At a given altitude, the averaging kernel is represented by the corresponding row of $\Phi$. However, $\Phi$ is not guaranteed to be positive and negative lobes may appear that make the interpretation of vertical resolution difficult. This was the case for ORA, probably due to the non-linearities of both measured signal and inversion method. Instead, we decided to re-write equation (14) as

$$(\beta(z) - \beta_0(z)) = \int_0^\infty \phi(z')(\beta_t(z') - \beta_0(z'))dz' \tag{15}$$

where the kernel function $\phi$ is constrained to be positive by choosing

$$\phi(z') = \frac{\gamma}{\delta\sqrt{\pi}} \exp(-(\frac{z' - z_*}{\delta})^2) \tag{16}$$

and $\gamma$, $z_*$ and $\delta$ are undetermined constants. At each altitude $z$, the equation (15) has been numerically solved in a least-squares sense with respect to $\gamma$, $z_*$ and $\delta$ for a large number of input and retrieved profiles in channel 5 ($\lambda$=600 nm). In Fig. 8, we present the value of $\delta(z)$ showing a good indication of the ORA vertical resolution which is about 2 km except below 20 km where it increases up to 5 km.

## 4 The Spectral Inversion Algorithm

Considering the acceptable quality of the vertical inversion, we restricted the spectral inversion to layers at $z_i = 10, 11, ...25, 27.5, ..50$ km (US standard atmosphere) and, for the time being, we discard channel 7 ($\lambda$ = 259 nm) which turned out to be defective and channel 4 ($\lambda$ = 943 nm) where water absorption requires a specific line-by-line calculation. In Fig. 9, we present the relative contributions of air, ozone and aerosol to the total extinction coefficient at $\lambda = 600$ nm.

A common problem encountered in the spectral inversion of UV-visible data is the interference of absorbing constituents that do not exhibit a very structured wavelength dependence. In other words, the measurement channels are not spectrally independent and an example of an extremely unfavourable case would be a $\lambda^{-4}$ aerosol dependence making it indistinguishable from Rayleigh scattering by air. Therefore, we decided to remove the air density by using assimilated data computed by the UKMO and suitably interpolated at the ORA tangent point (the estimated error grows roughly linearly from 1 % at 20 km to 2.5 % at 50 km).

Considering the set of total extinction coefficients at altitude $z_i$, one may write a system of linear equations relating the extinction by $O_3$, $NO_2$, and aerosols in the ORA channels as:

$$\begin{bmatrix} R_6^N & R_6^O & 1 & 0 & 0 & 0 & 0 & 0 \\ R_8^N & R_8^O & 0 & 1 & 0 & 0 & 0 & 0 \\ 1 & R_2^O & 0 & 0 & 1 & 0 & 0 & 0 \\ R_1^N & R_1^O & 0 & 0 & 0 & 1 & 0 & 0 \\ R_5^N & 1 & 0 & 0 & 0 & 0 & 1 & 0 \\ R_3^N & R_3^O & 0 & 0 & 0 & 0 & 0 & 1 \end{bmatrix} \cdot \begin{bmatrix} \beta_2^N \\ \beta_5^O \\ \beta_6^A \\ \beta_8^A \\ \beta_2^A \\ \beta_1^A \\ \beta_5^A \\ \beta_3^A \end{bmatrix} = \begin{bmatrix} \beta_6 \\ \beta_8 \\ \beta_2 \\ \beta_1 \\ \beta_5 \\ \beta_3 \end{bmatrix} \tag{17}$$

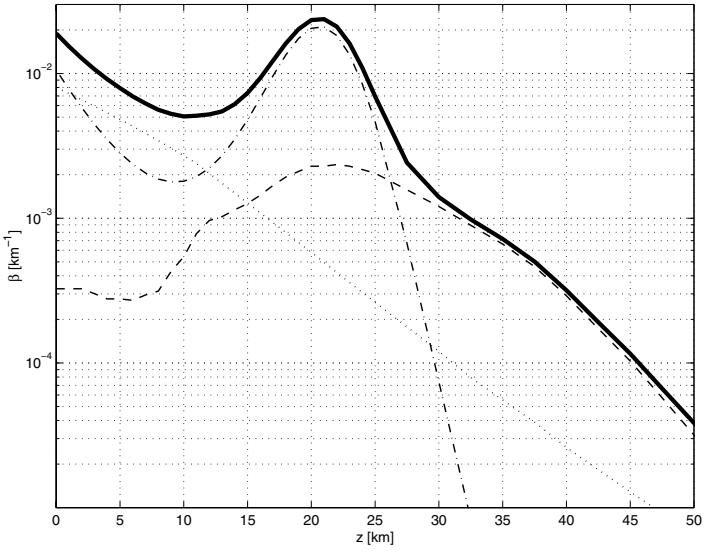


**Fig. 9.** Air(dotted), Ozone(dashed) and Aerosol(dash-dotted) extinction profiles with respect to total extinction (full line) at $\lambda = 600$ nm

or in matrix form:

$$A_i \cdot \overrightarrow{x_i} = \overrightarrow{\beta_i} \tag{18}$$

where $R_j^N = \sigma_j^N/\sigma_2^N$, $R_j^O = \sigma_j^O/\sigma_5^O$, and $\sigma_j^N, \sigma_j^O$refer to photoabsorption cross sections by respectively nitrogen dioxide and ozone in channel $j$, after convolution with the instrument function and $\beta_j^A$ stands for the aerosol extinction coefficient in channel $j$.

The aerosol wavelength dependence is a product of the spectral inversion contrary to absorption cross sections for ozone and nitrogen dioxide which are measured in the laboratory. By performing a simultaneous retrieval of ozone and nitrogen dioxide, the six available measurement channels $\{6, 8, 2, 1, 5, 3\}$ allow for 4 degrees of freedom for aerosol, which leads to exaggerated noise sensitivity. Keeping in mind, however, that broad extrema in the wavelength dependence have been observed after the Pinatubo eruption, we decided to describe the spectral behaviour of the aerosol extinction coefficient in channel $j$ as:

$$\beta_j^A(\lambda) = c_0 + c_1(\lambda_j - \lambda_3) + c_2(\lambda_j - \lambda_3)^2 \tag{19}$$

where the reference $\lambda_3 = 1013$ nm is the nominal wavelength of channel 3.

All cross sections have been taken from literature, and are assumed to be constant for all altitudes, except for $\sigma_6^O$, the ozone cross section at 340 nm (Higgins band absorption). Here we calculated an effective temperature for every altitude as a weighted average of all local UKMO temperatures along the slant path. The effective ozone cross section was then interpolated from

tabulated ozone data, using this effective temperature, and was convolved with the instrument function.

By using (19) under matrix form

$$\begin{bmatrix} \beta_2^N \\ \beta_5^O \\ \beta_6^A \\ \beta_8^A \\ \beta_2^A \\ \beta_1^A \\ \beta_5^A \\ \beta_3^A \end{bmatrix} = \begin{bmatrix} 1\,0\,0 & 0 & 0 \\ 0\,1\,0 & 0 & 0 \\ 0\,0\,1 & \lambda_6 - \lambda_3 & (\lambda_6 - \lambda_3)^2 \\ 0\,0\,1 & \lambda_8 - \lambda_3 & (\lambda_8 - \lambda_3)^2 \\ 0\,0\,1 & \lambda_2 - \lambda_3 & (\lambda_2 - \lambda_3)^2 \\ 0\,0\,1 & \lambda_1 - \lambda_3 & (\lambda_1 - \lambda_3)^2 \\ 0\,0\,1 & \lambda_5 - \lambda_3 & (\lambda_5 - \lambda_3)^2 \\ 0\,0\,1 & 0 & 0 \end{bmatrix} \cdot \begin{bmatrix} \beta_2^N \\ \beta_5^O \\ c_0 \\ c_1 \\ c_2 \end{bmatrix} \tag{20}$$

or

$$\overrightarrow{x_i} = K\ \overrightarrow{y_i} \tag{21}$$

the system (17) reduces to an overdetermined system of 6 equations with 5 unknowns. From inspection of the vertical inversion results, a small contribution of stray light, roughly proportional to $\lambda^{-4}$, was clearly visible. This straylight is measured, because the field of view of the instrument is much larger than the solar disk, and the instrument actually views the complete altitude range at every point during the course of the occultation. Because of this, we can assume that the straylight contribution is fairly constant during the occultation. We use this assumption instead of performing an explicit modelization of the straylight, which is an extremely difficult task. Therefore we write for the ensemble of 26 altitude levels:

$$\begin{bmatrix} A_1 & & & \overrightarrow{s} \\ & A_2 & & \overrightarrow{s} \\ & & \ddots & \vdots \\ & & A_{26} & \overrightarrow{s} \end{bmatrix} \cdot \begin{bmatrix} \overrightarrow{x_1} \\ \overrightarrow{x_2} \\ \vdots \\ \overrightarrow{x_{26}} \\ x_s \end{bmatrix} = \begin{bmatrix} \overrightarrow{\beta_1} \\ \overrightarrow{\beta_2} \\ \vdots \\ \overrightarrow{\beta_{26}} \end{bmatrix} \tag{22}$$

where

$$\overrightarrow{s} = \left(\lambda_6^{-4}\ \lambda_8^{-4}\ \lambda_2^{-4}\ \lambda_1^{-4}\ \lambda_5^{-4}\ \lambda_3^{-4}\right)^T \tag{23}$$

We rewrite the system (22) symbolically as:

$$A_{\mathrm{t}}\ \overrightarrow{x_{\mathrm{t}}} = \overrightarrow{\beta_{\mathrm{t}}} \tag{24}$$

The main reason for inverting all layers together is to regularize the solution at each layer by constraining it to be strongly correlated with the solution in the neighbouring layers. By using the a priori variance $\sigma^2\,(z_{i1})$ for a particular constituent, we constructed a vertical covariance matrix $C_{\mathrm{v}}$ with off-diagonal elements defined by:

$$\sigma^2\,(z_{i1}, z_{i2}) = \sqrt{\sigma^2\,(z_{i1})\,\sigma^2\,(z_{i2})} \cdot \exp\left(-\left(\frac{z_{i1} - z_{i2}}{L}\right)^2\right) \tag{25}$$

where a good trade-off between efficient regularization and oversmoothing is $L \simeq 5$ km. The exponential form is a Gaussian altitude correlation function[14]. Using

$$K_{\mathrm{t}} = \begin{bmatrix} K & & & \\ & \ddots & & \\ & & K & \\ & & & 1 \end{bmatrix} \tag{26}$$

and combining (21) and (24), we get:

$$A_{\mathrm{t}} K_{\mathrm{t}} \overrightarrow{y_{\mathrm{t}}} = B_{\mathrm{t}} \overrightarrow{y_{\mathrm{t}}} = \overrightarrow{\beta_{\mathrm{t}}} \tag{27}$$

and the a priori covariance matrix becomes

$$C_{\mathrm{z}} = (K_{\mathrm{t}}^T K_{\mathrm{t}})^{-1} K_{\mathrm{t}}^T C_{\mathrm{v}} K_{\mathrm{t}} (K_{\mathrm{t}}^T K_{\mathrm{t}})^{-1} \tag{28}$$

while the a priori vertical profiles $\overrightarrow{\tilde{x}_{\mathrm{t}}}$ lead to

$$\overrightarrow{\tilde{y}}_{\mathrm{t}} = (K_{\mathrm{t}}^T K_{\mathrm{t}})^{-1} K_{\mathrm{t}}^T \overrightarrow{\tilde{x}_{\mathrm{t}}} \tag{29}$$

Taking into account the data covariance matrix $C_{\mathrm{d}}$, the full least-squares problem (see [14]) reads

$$\left(B_{\mathrm{t}}^T C_{\mathrm{d}}^{-1} B_{\mathrm{t}} + C_{\mathrm{z}}^{-1}\right) \left(\overrightarrow{y_{\mathrm{t}}} - \overrightarrow{\tilde{y}}_{\mathrm{t}}\right) = B_{\mathrm{t}}^T C_{\mathrm{d}}^{-1} \left(\overrightarrow{\beta_{\mathrm{t}}} - B_{\mathrm{t}} \overrightarrow{\tilde{y}}_{\mathrm{t}}\right) \tag{30}$$

which has the solution

$$\overrightarrow{y_{\mathrm{t}}} = \overrightarrow{\tilde{y}}_{\mathrm{t}} + \left(B_{\mathrm{t}}^T C_{\mathrm{d}}^{-1} B_{\mathrm{t}} + C_{\mathrm{z}}^{-1}\right)^{-1} B_{\mathrm{t}}^T C_{\mathrm{d}}^{-1} \left(\overrightarrow{\beta_{\mathrm{t}}} - B_{\mathrm{t}} \overrightarrow{\tilde{y}}_{\mathrm{t}}\right) \tag{31}$$

associated with the posterior covariance matrix:

$$C_{\mathrm{p}} = \left(B_{\mathrm{t}}^T C_{\mathrm{d}}^{-1} B_{\mathrm{t}} + C_{\mathrm{z}}^{-1}\right)^{-1} \tag{32}$$

For $NO_2$ and $O_3$, we used an a priori variance of 50 percent with respect to the climatological a priori profile. This choice may seem rather arbitrary, but it ensures a positive solution in most cases, and, at the same time, provides a constraint that is not too tight.

For aerosols, the case is different. We cannot make use of a climatological profile, because the measurements were taken in the period following the Pinatubo eruption. We do know, however, that after removal of the Rayleigh component, only aerosol extinction is present in channel 3 (1013 nm), so we can use this as an a priori assumption. The a priori profiles at other wavelengths were evaluated, with (19), and the choice: $\tilde{c}_0 = \beta_3^A$, $\tilde{c}_1 = -2\beta_3^A$, and $\tilde{c}_2 = 2\beta_3^A$. This corresponds to a wavelength dependence that gradually increases with decreasing wavelength. The a priori variance at every wavelength is chosen to be 100 percent, to ensure that the constraint is not too tight.

The effect of this construction is that the regularization has practically no effect at the Junge layer level, only at high altitudes, where the solution for aerosol is unstable. It is important to realise that regularisation with covariance matrices is not strict. When assuming an a priori variance, this does not mean that the solution actually will be in this range. Only in the case when the merit function is broad and the solution is unstable, the prior knowledge will come into action.

## 5 Validation

As both experiments have a quite similar spectral range and number of channels, it was natural to compare ORA inverted profiles with SAGE II (see [8]) results. This validation has already been performed ([5]) for the total extinction profiles (however obtained by using the NOPE method alone). Furthermore, only three common channels could be used at that time. In the present comparison, we used the improved vertical inversion method (DM) and the above-described spectral inversion.

In order to assess a high degree of spatio-temporal coincidences between both experiments, we restricted the comparison domain at the tangent point to six minutes in time and two degrees in latitude or longitude. As only 25 ORA /SAGE occultations satisfy this constraining criterion, they are expected to actually observe the same atmospheric situation (see [5] for a more detailed discussion of the comparison statistics).

For all constituents, we used a linear interpolation scheme to evaluate the SAGE II data at the ORA altitude levels. The errors have been calculated through combination of the statistical variance of the 25 profiles with the individual profile errors:

$$\epsilon^2 = \frac{\sum (p_i - \bar{p})^2}{n} + \frac{\sum \epsilon_i^2}{n} \tag{33}$$

with $p_i$ and $\epsilon_i$ the i-th profile and its error, respectively. The relative difference between the two experiments is evaluated as $100 \times (ORA - SAGE)/SAGE$.

The results for ozone and $NO_2$ are depicted in Fig. 10. Data for SAGE II were only available in the altitude range from 20 to 50 km. For ozone, the difference is at most 40 percent. The $NO_2$ profiles are also in fair agreement, except at lower altitudes, where the ORA mean profile is abnormally large. The main reason is probably the coupling between the aerosols and $NO_2$ during the spectral inversion, because the spurious peak of the $NO_2$ profile occurs at the same altitude as the aerosol peak. Also, this is an altitude region where the relative contribution of $NO_2$ to the total extinction is very low, compared to other constituents.

On the other hand, the SAGE II team recently announced a reprocessing of their data at the algorithm level 6.0. It is worth noting that the finite UV-visible spectral range of both experiments is responsible for an irreducible

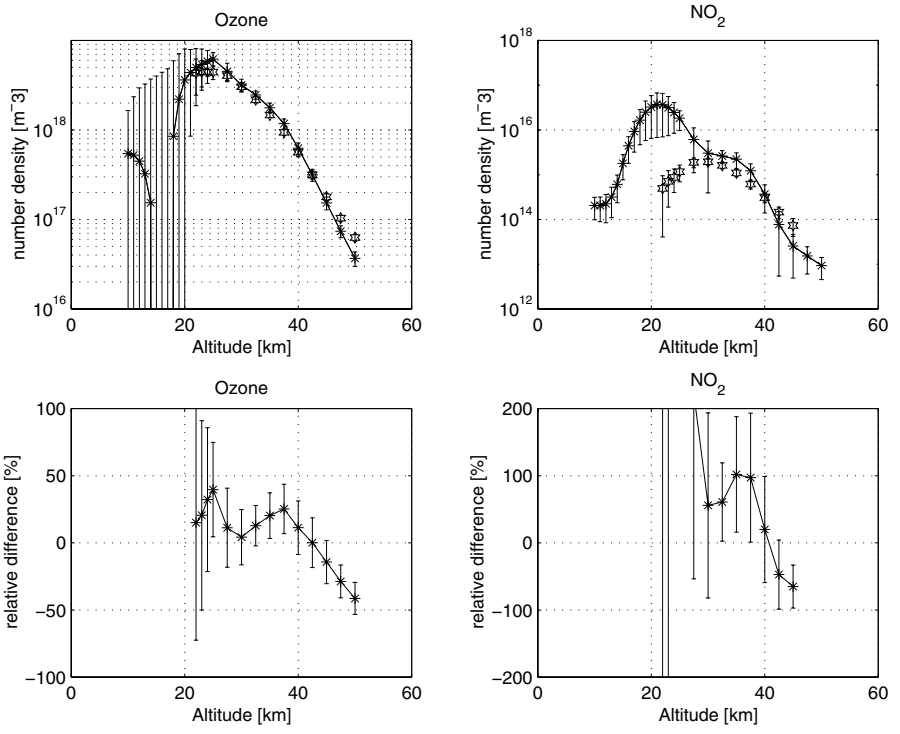


**Fig. 10.** Top: Comparison between mean ORA ( asterisks connected by full line) and SAGE (stars) profiles for ozone and $NO_2$. Bottom: Mean of relative differences.

coupling between constituents. In the extreme case of an aerosol extinction coefficient that would behave like the ozone cross section, it would be impossible to make the distinction between aerosol and ozone contents.

The aerosol optical thickness is calculated as the upwards integrated extinction, with respect to a reference altitude level. Many authors [15, 3] take this level to be 2 km above the local tropopause level. This choice is the result of two considerations. First, it is supposed to reasonably prevent the optical thickness to be affected by possible clouds. Secondly, the altitude surfaces of equal aerosol extinction roughly 'follow' the global tropopause surface.

We calculated the tropopause level for every ORA event from United Kingdom Meteorological Office (UKMO) temperature profiles, using the standard definition of tropopause, but noticed a variability of several kilometers for different events at identical latitudes and months. While this variability reflects the local meteorological state, we realized that it could cause unwanted side effects in the optical thickness computation. Because of this, we preferred to use the monthly mean values of tropopause altitude. Other authors have also encountered this problem and used a similar remedy [3].

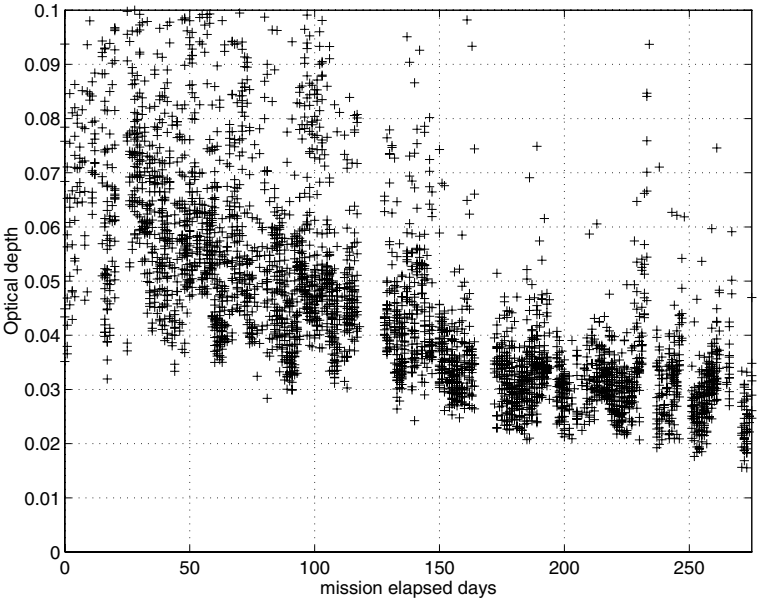


**Fig. 11.** Total vertical optical thickness measured by ORA at $\lambda = 1013$ nm

Taking this into account, the aerosol optical thickness at 1013 nm is calculated as:

$$\delta_a = \int_{z_{\mathrm{ref}}+2} \beta_3^A(z)\, dz \tag{34}$$

with $z_{\mathrm{ref}} = z_{\mathrm{T}} + 2$ km, and $z_{\mathrm{T}}$ equals the local tropopause altitude level, interpolated from mean values, tabulated as function of month and latitude.

It was clear from the start of the data processing that a considerable number of the ORA extinction profiles showed abnormally high values at low altitudes. Taking into account that these outliers would distort the final geophysical processing results, we decided to remove them by applying a statistical rejection criterium. After this procedure, 4547 events were left. A first comparison of the 2274 rejected events with monthly mean cloud coverage maps obtained from the International Satellite Cloud Climatology Project (ISCCP) showed that a high probability of cloud occurrence can be associated with these events.

Further investigation revealed another suspicious behaviour. We observed a decrease in time, explained by the gradual sedimentation and dispersion of aerosols, but at the same time, the variability of the optical thickness increased. This could not have been caused by the inversion algorithm, because the same increase of variability was observed in the raw transmission signals at low altitudes. We soon realised that the effect was caused by additional light extinction by smaller subvisual clouds. The presence of such a cloud does not produce a radical cut-off in the measured signal, but introduces a

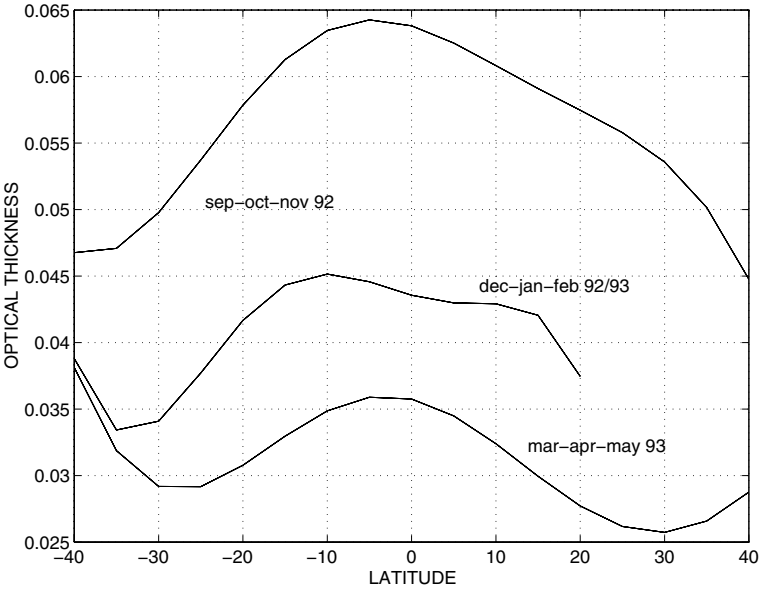


**Fig. 12.** Total vertical optical thickness measured by ORA at $\lambda = 1013$ nm

modulation in the measured transmission. So the random cloud relative modulation increases with decreasing aerosol extinction and associated increasing transmission, as observed.

The cause for this cloud modulation at stratospheric altitudes is of course the large field of view of the ORA optical modules. Two kilometers above tropopause altitude, the instrument is still capable of viewing tropospheric clouds.

## 6 Conclusions

The NOPE vertical inversion algorithm was used to calculate total extinction profiles for 7000 occultation events. Furthermore, the Direct Method (DM) was able to improve these profiles at altitudes where the measured transmission was almost zero or one, or when the fit between measured and modelled transmission was not optimal. The DM method is a simple nonlinear mapping between measured transmission and total extinction, and is therefore very straightforward to calculate.

The separation of species, or spectral inversion, was performed with the aid of a least squares method, using a priori covariance information. The resulting altitude profiles for $O_3$, $NO_2$ and aerosols were in satisfactory agreement with the data obtained with the SAGE II experiment. At lower altitudes, in a region where SAGE II could not produce good data (signal

cut-off), ORA was able to deliver aerosol extinction data. This shows that it is possible to obtain quality data with a low-cost instrument, equipped with very simple optics.

**Acknowledgments**

We would like to thank the United Kingdom Meteorological Office (UKMO), that provided us with the assimilated pressure and temperature data sets. This work was partly performed within the project "Measurement, understanding and climatology of stratospheric aerosols" funded by the SSTC/ DWTC service of the Belgian Government.

## References

1. E. Arijs, D. Nevejans, D. Fussen, P. Frederick, E. Van Ransbeek, F. W. Taylor, S. B. Calcutt, S. T. Werrett, C. L. Heppelwhite, T. M. Pritchard, I. Burchell, and C.D.Rodgers. The ORA Occultation Radiometer on EURECA. *Advances in Space Research*, 16:833–836, 1995.
2. Max Born and Emil Wolf. *Principles of Optics*. Pergamon Press, Oxford, 1993.
3. C. Brogniez and J. Lenoble. Analysis of 5-year Aerosol Data From the Stratospheric Aerosol and Gas Experiment. *Journal of Geophysical Research*, 96:15479–15497, 1991.
4. W. P. Chu, M. P. McCormick, J. Lenoble, C. Brogniez, and P. Pruvost. SAGE II Inversion Algorithm. *Journal of Geophysical Research*, 94:8839–8351, 1989.
5. D. Fussen, E. Arijs, D. Nevejans, F. Van Hellemont, C. Brogniez, and J. Lenoble. Validation of the ORA spatial inversion algorithm with respect to the stratospheric aerosol and gas experiment II data. *Applied Optics*, 37:3121–3127, 1998.
6. D. Fussen, E. Arijs, D. Nevejans, and F. Leclere. Tomography of the Earth's Atmosphere by the Space-Borne ORA Radiometer: Spatial Inversion Algorithm. *Journal of Geophysical Research*, 102:4357–4365, 1997.
7. O. K. Garriott. Visual Observations From Space. *J. Opt. Soc. Am.*, 69:1064–1068, 1979.
8. J. Lenoble. Presentation of the European Correlative Experiment Program for SAGE II. *Journal of Geophysical Research*, 94:8395–8398, 1989.
9. Mauldin III L. E., N. H. Zaun, M. P. McCormick, J. H. Guy, and W. R. Vaughn. Stratospheric Aerosol and Gas Experiment II Instrument: A Functional Description. *Opt. Eng.*, 24:307–312, 1985.
10. W. H. Press, S. A. Teukolsky, W. T. Vetterling, and B. P. Flannery. *Numerical Recipes in FORTRAN, Second Edition*. Cambridge University Press, Cambridge, 1992.
11. R. G. Roble and P. B. Hays. A Technique for Recovering the Vertical Number Density Profile of Atmospheric Gases From Planetary Occultation Data. *Planetary Space Science*, 20:1727–1744, 1972.
12. C. D. Rodgers. Retrieval of Atmospheric Temperature and Composition From Remote Measurements of Thermal Radiation. *Reviews of Geophysics and Space Physics*, 18:609–624, 1976.

13. C. D. Rodgers. Characterization and Error Analysis of Profiles Retrieved From Remote Sounding Measurements. *Journal of Geophysical Research*, 95:5587–5595, 1990.
14. A. Tarentola. *Inverse problem theory.* Elsevier, Sara Burgerhartstraat, 25, P. O. Box 211, 1000 AE Amsterdam, The Netherlands, 1987.
15. C. R. Trepte, L. W. Thomason, and G. S. Kent. Banded structures in stratospheric aerosol distributions. *Geophysical Research Letters*, 21:2397–2400, 1994.